Differential laboratory passaging of SARS-CoV-2 viral stocks impacts the in vitro assessment of neutralizing antibodies

Aram Avila-Herrera[1], Jeffrey A. Kimbrel[2], Jose Manuel Marti[1], James Thissen[2], Edwin A. Saada[2], Tracy Weisenberger[2], Kathryn T. Arrildt[2], Brent Segelke[2], Jonathan E. Allen[1], Adam Zemla[1], and Monica K. Borucki[2]*

[1]Lawrence Livermore National Laboratory, Computing Directorate, Global Security Computing Division, Livermore, CA, United States of America.

[2]Lawrence Livermore National Laboratory, Physical and Life Sciences Directorate, Biotechnology and Biosciences Division, Livermore, CA, United States of America.

*Correspondence: borucki2@llnl.gov

Keywords: SARS-CoV-2; laboratory passage; neutralization; monoclonal antibody; mutation; variant; epitope; binding affinity

18 Abstract: Viral populations in natural infections can have a high degree of sequence diversity,
19 which can directly impact immune escape. However, antibody potency is often tested in vitro
20 with a relatively clonal viral populations, such as laboratory virus or pseudotyped virus stocks,
21 which may not accurately represent the genetic diversity of circulating viral genotypes. This can
22 affect the validity of viral phenotype assays, such as antibody neutralization assays. To address
23 this issue, we tested whether recombinant virus carrying SARS-CoV-2 spike (VSV-SARS-CoV-2-S)
24 stocks could be made more genetically diverse by passage, and if a stock passaged under
25 selective pressure was more capable of escaping monoclonal antibody (mAb) neutralization
26 than unpassaged stock or than viral stock passaged without selective pressures. We passaged
27 VSV-SARS-CoV-2-S four times concurrently in three cell lines and then six times with or without
28 polyclonal antiserum selection pressure. All three of the monoclonal antibodies tested
29 neutralized the viral population present in the unpassaged stock. The viral inoculum derived
30 from serial passage without antiserum selection pressure was neutralized by two of the three
31 mAbs. However, the viral inoculum derived from serial passage under antiserum selection
32 pressure escaped neutralization by all three mAbs. Deep sequencing revealed the rapid
33 acquisition of multiple mutations associated with antibody escape in the VSV-SARS-CoV-2-S that
34 had been passaged in the presence of antiserum, including key mutations present in currently
35 circulating Omicron subvariants. These data indicate that viral stock that was generated under
36 polyclonal antiserum selection pressure better reflects the natural environment of the
37 circulating virus and may yield more biologically relevant outcomes in phenotypic assays.

38

Keywords: SARS-CoV-2; laboratory passage; neutralization; monoclonal antibody; mutation; variant; epitope; binding affinity

1. Introduction

Severe acute respiratory syndrome coronavirus 2 (SARS-CoV-2) has been notably efficient at rapidly evolving resistance to monoclonal antibodies (mAbs) by producing versions of the spike protein with a diversity of amino acid changes that interfere with antibody binding. Importantly, the increased genetic diversity of viral populations that are generated within immunocompromised hosts threatens the efficacy of antibody treatments that are a vital resource for this vulnerable population (1-3). Neutralization assays performed to identify antibody escape mutants generally use a laboratory stock of SARS-CoV-2 strain or a pseudotyped or chimeric virus with a spike protein that represents the wild type Wuhan-Hu-1 strain (3). Passage of viruses in established laboratory cell lines is a convenient way to maintain viral stocks, however the impact of laboratory passage on the genetic diversity of rapidly mutating virus may skew the results of experiments (4-7). While this enables comparison of results between studies, this laboratory stock may not reflect the genetic diversity of circulating strains of the virus.

In this study we passaged a replication-competent vesicular stomatitis virus (VSV) expressing a modified form of the SARS-CoV-2 spike protein (VSV-SARS-CoV-2-S) (8) in three different cell lines and then with or without antiserum selection pressure (Figure 1). Because VSV is an RNA virus and thus has a highly error-prone RNA-dependent RNA polymerase, passage of the spike

60 protein in the VSV backbone rapidly generates mutations in the spike protein during replication
61 (9). We hypothesized that this type of passage would increase the genetic diversity of the viral
62 spike protein and enable the virus to more readily escape antibody neutralization as compared
63 to virus passaged without selection pressure.

64 The SARS-CoV-2 spike protein consists of two subunits, S1 and S2. The S1 subunit binds to a
65 host cell receptor and includes two regions important for antibody evasion, the N-terminal
66 domain (NTD), and the receptor-binding domain (RBD). The S2 subunit is separated from the S1
67 subunit by a furin cleavage site and functions in virus-cell membrane fusion. To identify
68 mutations associated with passage and antibody escape, the VSV-SARS-CoV-2-S spike gene was
69 deep sequenced prior to passage, after passage in different cell lines, after passage under
70 antiserum selection, and after mAb escape (Figure 1). The mutations that were detected after
71 passage and selection pressure were analyzed using epitope analysis and protein structural
72 modeling.

73

74 *Figure 1. Virus passage and assay workflow. Cell lines and assay components are in boxes, viral inocula are in ovals. UP:*
75 *unpassaged virus; SEQ: samples were deep sequenced; VERO-TMP: VERO/TMPRSS2; P4 mix: mixture of virus from passage 4 all*
76 *cell lines; VO: virus only (no antibody selection), VA: virus passaged in the presence of antibody (antiserum from vaccinated*
77 *individuals).*

78 The cell lines chosen for passage are cell lines commonly used for propagation of coronaviruses
79 that have previously been shown to impact virus mutation (7, 10, 11). Vero and Vero/TMPRSS2
80 cell lines are highly susceptible to SARS-CoV-2 and generate high viral titers, whereas Calu-3
81 and Caco-2 cells represent cell types found in biologically relevant tissues, the human

82 respiratory tract and human gastrointestinal tract, respectively, but SARS-CoV-2 may grow to
83 lower titers in these cell lines (7, 12).
84

85 2. Materials and Methods

86 2.1 Virus. A replicating VSV-SARS-CoV-2-S virus (recombinant virus VSV-SARS-CoV-2-S SΔ21, a
87 gift from Sean Whelan laboratory, Univ. of Washington), which expresses eGFP and has a stop
88 mutation at spike residue 1253 was used for analysis of mutations associated with cell passage
89 and antibody escape (8). Stock VSV-SARS-CoV-2-S virus was generated by passaging once in
90 Vero/TMPRSS2 cells (a gift from Sean Whelan lab, Univ of Washington) at an MOI of 0.05 (as
91 determined by TCID50 assay). The stability of the virus genotype after passage was confirmed
92 via Sanger sequencing and by Illumina sequencing. No changes in the consensus sequence were
93 detected.

94 2.2 Cell lines. The following cell lines were used for passage of the virus: Vero-TMPRSS2 cells,
95 Caco-2 Human intestinal cells (ATCC HTB-37), Vero E6 African Green Monkey kidney cells (ATCC
96 CRL-1586), and Calu-3 Human lung epithelial (ATCC HTB-55). The cell lines were propagated in
97 DMEM media supplemented with 1% Penicillin/Streptomycin and 5 – 10% fetal bovine serum.

98 2.3 Antiserum and monoclonal antibodies. Polyclonal antiserum, Pooled Human Serum
99 Sample, Pfizer Vaccine (NRH-17727) (13), was obtained from BEI Resources. Human Anti-SARS-
100 CoV-2 Spike-RBD Clone S309 mAb and Human Anti-SARS-CoV-2 Spike-RBD REGN10987 mAb

101 (Imdevimab) were purchased from Cell Sciences (Newburyport MA, USA). 2130-1-0114-112
102 (LLNL-112) is an antibody developed at LLNL (14) derived from COV2-2130 or ciglavimab (15).

103 2.4 Passage on cell lines. Virus was serially passaged four times on three different cell lines to
104 determine whether different mutations are generated in different cell lines. "Unpassaged"
105 stock virus (UP) was used to infect Vero, Vero/TMPRSS2, Caco-2 and Calu-3 cell lines at an MOI
106 of 0.25. After 48h the supernatant was collected and clarified (1000 x g for 5 min) and 100 µl of
107 the supernatant was used for the subsequent passage experiments.

108 2.5 Passage in presence of polyclonal antiserum. To increase the genetic diversity of viral
109 preparations, diluted polyclonal antiserum (Pooled Human Serum Sample, Pfizer Vaccine NRH-
110 17727) was incubated with viral preparations for 1h at 37 °C (Table 1). One hundred microliters
111 of virus-antibody mixtures were used to infect Vero/TMPRSS2 cells in 6-well plates (9). After
112 48h the two wells with the lowest dilution of antiserum were combined for the next passage.
113 Virus was also passaged without antiserum present to differentiate mutations due to serial
114 passage from mutations due to antibody selection pressure. In each case, virus was serially
115 passaged for a total of six passages.

116 2.6 Neutralization assay. To determine whether passage history (cell line and antibody
117 selection pressure) enabled mutant escape of monoclonal antibodies, dilutions of monoclonal
118 antibodies (10 µg/ml or 5 µg/ml) were incubated with 5 × 104 infectious units of virus for 1 hr
119 at 37 °C then applied to monolayers (90% confluence) of Vero/TMPRSS2 cells in 96-well plates
120 in duplicate wells. Supernatant from duplicate wells were pooled for sequence analysis. Three
121 different monoclonal antibodies were tested: S309, REGN10987, and mAb LLNL-112.

122 2.7 RT PCR. RNA was extracted from 140 µl of culture supernatant using the Qiagen QIAamp
123 Viral RNA Mini Kit. Viral RNA was amplified and sequenced using a version of the ARTIC
124 protocol, nCoV-2019 sequencing protocol (https://www.protocols.io/view/ncov-2019-
125 sequencing-protocol-v3-locost-bp2l6n26rgqe/v3, accessed 12/22/2022). Because the spike
126 gene may mutate rapidly, the spike gene was amplified using two ARTIC primer sets, v3 and 4.1
127 to increase the chance of mutations being detected. All of the samples with exception of cell
128 passage 1 and 4 (Figure 1) were amplified in duplicate PCR reactions, thus for each of these
129 samples 8 different PCR reactions were performed (each ARTIC primer set requires 2 different
130 PCR reactions and two ARTIC primer versions were used in replicates). The RT reaction was
131 performed using the Luna (NEB). The cDNA was amplified in a 25 µl PCR reactions using 6 µl
132 cDNA and 2X Master mix (NEB). The PCR cycling program was 98 °C for 30 seconds, then 35
133 cycles of 98 °C for 15 seconds, 65 °C for 5 minutes. A negative PCR control for each PCR set was
134 prepared using PCR grade water as a template. Negative control PCR products were combined
135 from different PCR batches and was sequenced as a negative control. The PCR products from
136 each reaction were pooled then were purified using AMPureXP beads (Beckman Coulter, Brea,
137 CA, USA). A negative control (no template control, NTC) was prepared by pooling the NTC PCR
138 products from multiple runs from each primer set.

139 2.8 Sequencing. A total of 40 µL of pooled v3 and v4.1 ARTIC amplicons were purified by
140 adding 0.8X of Ampure XP magnetic beads (Beckman Coulter) to each pooled amplicon sample.
141 The PCR products were purified following the standard manufacturer's instructions and
142 resuspended in 22 µL of water. The purified PCR products were quantified using the Qubit
143 fluorimeter (ThermoFisher) and 100 ng of each sample was input into the Illumina DNA Prep

144 library kit (Illumina). The small amplicon manufacturer's instructions were followed for the
145 library kit and completed libraries were quantified and verified on the Tapestation 4200
146 instrument (Agilent). The completed libraries were diluted to 4 nM, pooled, and further diluted
147 to a loading concentration of 8 pM. The libraries were sequenced on the Illumina MiSeq
148 instrument using a v2 2x250 sequencing kit. Raw sequencing data has been uploaded to the
149 NCBI under BioProject PRJNA978027.

150 2.9 Bioinformatic analysis. Variants were called using Mappgene,
151 (https://github.com/LLNL/mappgene) a SARS-CoV-2 variant calling pipeline for high
152 performance computing environments (HPC) (16). Mappgene employs BWA-MEM (17) for read
153 alignment, iVar 1.3.1 for read trimming/filtering/variant calling, and LoFreq v2.1.5 to call
154 variants (18).

155 2.10 Epitope analysis. The epitope regions for three SARS-CoV-2 neutralizing antibodies and
156 the hACE2 receptor binding motif (RBM) were modeled to determine if epitopes are in close
157 proximity or overlapping the RBM, and if the locations of the observed mutations might impact
158 binding (Figure 2). The coordinates for the S309-RBD complex comes from PDB entry 7R6W; the
159 Regeneron REGN10987-RBD complex from PDB entry 6XDG (chains A and C make up the
160 REGN10987 light and heavy chain, respectively, Fab complexed with RBD [chain E]); and the
161 LLNL-112-RBD complex comes from a model structured generated at Lawrence Livermore
162 National Laboratory (LLNL) which was in turn produced from the COV2-2130 complex with RBD
163 coordinates in PDB entry 7L7E. The RBM was determined from the human ACE2-SARS-CoV-2
164 RBD complex coordinates in PDB entry 6M0J. The amino acids making up the epitopes and RBM
165 were determined from the listed coordinate sets as described and the region made up of these

166 residues is outlined on the RDB molecular surface from PDB entry 7R6W; the epitopes and RBM
167 were outlined on a common RBD molecular surface for ease of comparison.

168 2.11 Protein structural analysis. To assess if the escape mutations increased ability to evade
169 neutralizing antibodies, we applied our Structural Fluctuation Estimation (SFE) method (19) to
170 predict their impact on different mAbs in complex with the Wuhan as well as the Omicron
171 strains. To make more complete comparison, the estimations of binding affinity changes (ΔΔG -
172 predicted changes in binding energy upon introduced mutations) were also calculated for the
173 RBD-ACE2 complexes (19). SFE starts with the construction of structural models for each of the
174 RBD-mAb and RBD-ACE2 complexes. For each constructed complex we performed minimization
175 and relaxation using disparate approaches: Rosetta (20), Chimera (21), and GROMACS (22)
176 steepest decent and conjugant gradient minimizations, and molecular dynamics trajectories
177 from GROMACS simulations. This procedure as applied to each of constructed complexes
178 allowed us to sample an extended number of structural conformations, use them to perform
179 "forward" and "reverse" ΔΔG calculations using Flex ddG (23), remove outliers, average results,
180 and report with higher confidence final energy change estimates. By computing ΔΔG's across
181 many conformations of each constructed complex, we reduced uncertainties in the structural
182 modeling and estimated natural conformational fluctuations within the complexes.

183 3. Results

184 3.1 Virus passage on different cell lines. To determine the effect of host cell line on viral
185 diversity, virus was passaged four times on different cell lines: Vero, Vero/TMPRSS2, Caco-2 and
186 Calu-3. Unpassaged stock virus (UP) was used to infect each cell lines at an MOI of 0.25. After

187 48 h the supernatant was collected and 100 µl of the supernatant was used to for the
188 subsequent passage experiments. This was repeated for a total of 4 passages per cell line with
189 the exception of Calu-3 cells. Calu-3 cells had no cytopathic effect (CPE) evident after 48 h post
190 infection and few cells expressing GFP per field after the first passage. No GFP expression or
191 CPE was observed in passage 2 of the Calu-3 cells. The 2nd passage was repeated a total of 3
192 times with the same result. Calu-3 cells over expressing human ACE-2 receptor was obtained
193 from BEI Resources (Clone 2B4, NR-55340) and passage was tried using this cell line with no
194 evidence of CPE or GFP expression, although inoculation of Calu-3 passage 1 (P1) supernatant
195 onto Vero/TMPRRS2 cells did yield strong GFP expression.

196 After 4 passages in Vero, Vero/TMPRSS2, or Caco-2 cells, supernatant from the final passage in
197 each cell line was titered by TCID50 and equal amounts of passaged virus (2 x 105infectious
198 units) were combined into a single inoculum for subsequent passages under antibody selection
199 pressure.

200 3.2 Virus passage with antibody selection pressure. To understand how antibody selection
201 pressure can modify the mutational profiles, this "Cell-passaged" inoculum was used to infect
202 Vero/TMPRSS2 cells at an MOI of 0.1 in the presence of polyclonal antiserum ("Virus and
203 antibody", VA) or in media without the presence of polyclonal antiserum ("Virus only", VO). For
204 passage in the presence of sera, three different dilutions of antisera were used per passage,
205 and supernatant from the two lowest dilutions showing CPE and expressing GFP were collected
206 and combined for the subsequent passage. Early passages showed that highly diluted sera did
207 not inhibit viral growth thus sera concentrations were increased in subsequent passages (Table
208 1).

209

Passage	Dilution 1	Dilution 2	Dilution 3	Dilutions with GFP/CPE	Dilutions collected
1	1:100	1:200	1:400	All	1 and 2
2	1:50	1:100	1:200	All	1 and 2
3	1:10	1:20	1:50	All	1 and 2
4	1:5	1:10	1:20	All	1 and 2
5	1:5	1:10	1:20	All; 1:5-GFP but little CPE	1 and 2
6	1:5	1:10	1:20	All; 1:5-GFP but not CPE	1 and 2

210 ***Table 1.*** *Antiserum dilutions used and collected per passage for selection pressure. Three different dilutions of antiserum were*
211 *used per passage (1-6) in Vero/TMPRSS2 cells. The supernatant from the two lowest dilutions showing CPE and expressing GFP*
212 *were collected and combined for the subsequent passage. Passage 6 dilutions 1:10 and 1:5 were combined for use in the*
213 *neutralization assay. GFP: Green fluorescent protein; CPE: Cytopathic effect*

214 ### 3.3 Genetic analysis of mutations associated with cell passage and antiserum selection
215 pressure. To identify mutations associated with passage in cell lines and in the presence of
216 antiserum, the spike gene within the VSV backbone was amplified using multiplexed PCR (ARTIC
217 V3 protocol) and sequenced using the Illumina platform. The UP stock and passaged samples
218 (VO, VA) were PCR amplified and sequenced in duplicate to increase confidence in detection of
219 low frequency mutations. The ARTIC primer sets are designed to span the genome (versus just
220 the spike gene), and the highly multiplexed primer sets amplified 97% of the spike gene present
221 in the VSV vector and did not appear to be negatively impacted by the presence of primers
222 designed to amplify other regions of the SARS-CoV-2 genome. Although the RT-PCR amplicons
223 often produced many bands larger than the target size of 400 bp, sequencing coverage was
224 excellent with >95% of the spike gene having coverage of at least 1000 x depth (Supp data Fig
225 1). None of the negative control samples showed bands of any size on the PCR gels. The first
226 sequencing run had a maximum of 11 reads mapped to any nt position for the negative PCR
227 control (NTC), the second run had no mapped reads from the NTC.

228 Analysis of the deep sequence data revealed no mutations were detected at >1% frequency in
229 the UP stock (sequenced in duplicate). A high frequency mutation, R685S, was detected in Vero
230 P1 at 5.2% and at 83.8% frequency in Vero passage 4 (P4) (Table 2). Interestingly, VSV-GFP-
231 SARS-CoV-2-S Δ21 with the R685S mutation has previously been isolated from WT stock (24).
232 Four mutations were detected in Vero/TMPRSS2 P4 and these mutations were enriched in later
233 samples, often at much higher frequencies: L48S, T76I, H655Y, and I1081V (Tables 2 and 3,
234 Supp Table 3). Caco-2 P4 had only one mutation detected at >1%, I468T detected at 2.2%
235 frequency (Table 2).

236

NT POS	SAMPLE	ALT FREQ	TOTAL DP	REF AA	ALT AA	AA POS
22148	Vero P1	1.5%	24676	N	A	196
22217	Vero P1	1.5%	27925	G	R	219
22221	Vero P1	1.5%	25686	F	S	220
23615	Vero P1	5.2%	61047	R	S	685
24371	Vero P1	1.0%	51215	S	T	937
25135	Vero P1	1.1%	19448	K	N	1191
21639	Vero P4	1.1%	2062	P	L	26
23280	Vero P4	1.4%	22686	T	I	573
23615	Vero P4	83.8%	24956	R	S	685
24519	Vero-T P1	1.1%	41172	K	T	986
24725	Vero-T P1	1.2%	41352	S	T	1055
21705	Vero-T P4	1.3%	10070	L	S	48
21789	Vero-T P4	11.7%	12269	T	I	76
23525	Vero-T P4	2.5%	95426	H	Y	655
24725	Vero-T P4	1.1%	44127	S	T	1055
24803	Vero-T P4	2.0%	36361	I	V	1081
21900	Calu P1	1.4%	7314	K	M	113
23889	Calu P1	1.4%	60152	K	R	776
22965	Caco P4	2.18%	46755	I	T	468

237 ***Table 2.*** *Mutations detected after passage in cell lines. Abbreviations Vero-T: Vero/TMPRSS2; NT POS: Nucleotide position in the*
238 *reference sequence Wuhan-Hu-1 (NC_045512.2); AVG FREQ: Average frequency; TOTAL DP: Depth of sequence read coverage*
239 *for the nt pos; REF AA: Amino acid in the reference sequence; ALT AA: Amino acid in the sample sequence; AA POS: Residue*
240 *number in the spike gene.*

241 After pooling equal amount of virus (P4) from the three cell lines (Fig 1), the virus was further
242 passaged six times in Vero/TMPRSS2 cells either with or without the presence of antiserum.

243 Viral RNA from passage 6 was PCR amplified in duplicate and subjected to deep sequencing.

244 Table 3 shows the location and frequency of the mutations detected.

245 The six passages with or without antiserum selection pressure induced high frequency

246 mutations in three residues, T76I, H655Y, and I1081V, with H655Y and I1081V appearing to be

247 linked due to these mutations always being detected together and at the same approximate

248 frequency. These mutations were first detected in Vero/TMPRSS2 P4. Interestingly, virus

249 passaged six times without antiserum selection pressure (VO-P6) produced a high frequency

250 mutation, I569S that continued to persist at high frequency exclusively in virus only samples,

251 and was not detected in samples passaged in the presence of antiserum or mAbs (Table 3, Supp

252 Table 3). Alternatively, the three mutations that were located in the RBD were detected only in

253 samples passaged in the presence of antiserum (VA-P6) or mAbs.

254

Sample ID	Antiserum or mAb	L48S	T76I	H245Y	Y248N	E340A	R346S	K444N	K444T	G446V	Q493R	I569S	H655Y	L977F	N978K	S982L	V991A	I1081V
CELL PASSAGE																		
UP	None																	
VERO P4	None																	
VERO-T P4	None	1.3	11.7										2.5					2.0
CACO P4	None																	
ANTISERUM PRESSURE																		
VO-P6	None	1.8	12.0									9.7	82.0				1.3	84.4
VA-P6 (1:5)	Antiserum		37.4		1.6		1.4				1.7		74.3					75.5
VA-P6 (1:10)	Anitserum		24.0										47.1					49.3
NEUTRALIZATION ASSAY																		
mAB LLNL-112																		
UP	LLNL-112 (5 µg/ml)																	
VO-P6	LLNL-112 (5 µg/ml)	1.8	12.9									8.8	83.1				1.2	83.2
VA-P6	LLNL-112 (5µg/ml)		8.6				56.7						88.9					89.1
VA-P6	LLNL-112 (10 µg/ml)		60.9					52.2			58.4		33.8					36.0
mAb REGN10987																		
UP	REGN10987 (5 µg/ml)																	
VO-P6	REGN10987 (5 µg/ml)	4.0	11.6									9.7	83.1			1.1	2.0	83.1
VA-P6	REGN10987 (5 µg/ml)		20.0	15.7	17.2			31.2	16.0	40.8	16.0		80.3					82.1
mAb S309																		
UP	S309 (5 µg/ml)																	
UP	S309 (10 µg/ml)																	
VO-P6	S309 (5 µg/ml)		3.7									46.6	90.0	18.0	5.7			90.0
VO-P6	S309 (10 µg/ml)	5.1	8.3									41.5	89.3			14.0	16.0	90.0
VA-P6	S309 (5 µg/ml)		10.1			57.1	1.1						87.6					88.7
VA-P6	S309 (10 µg/ml)		13.6		1.2	30.0					1.1		83.1					84.0

255 ***Table 3.*** *Comparison of variant frequencies associated with cell culture passage, passage under antiserum selection, and mAb*

256 *selection. Mutations that are present in at least 1 sample at > 5% are shown and that are present in antiserum passaged*

257 *samples and/or neutralization data are shown (see Suppl Table 1 for mutations present at 1% or greater). Note cell passaged*

258 *samples from Vero and Caco-2 cells did not have mutations that persisted and are not shown. Antiserum passaged samples (VA-*

259 *P6) have serum dilution (1:5 or 1:10) shown in parentheses. Samples that were tested with the neutralization assay are denoted*

260 *by the mAb name, the viral inoculum (UP, VO-P6, or VA-P6), and the mAb concentration (5 µg/ml, 10 µg/ml). Data from virus*

261 *only passaged samples (no antibody selection) are shown in blue cells and data from virus passaged under antiserum or mAb*
262 *selection are in yellow shaded cells. Top row cells shaded grey signify columns with data from both virus only and antibody*
263 *selection. With the exception of Vero P4, Vero-T P4 and Caco P4, all samples were processed (PCR and sequencing) in duplicate;*
264 *the percent frequency is an average of the two values.*

265 3.4 Mutations associated with escape from mAb neutralization. To determine whether the
266 mutations that occurred during passage with antiserum selection pressure could confer
267 resistance to mAbs designed to treat COVID infections, supernatant from UP, VA-P6, and VO-P6
268 were assayed for mAb escape using neutralization assays and deep sequencing (Figure 1).

269 mAbs (5 µg/ml and 10 µg/ml) were incubated with 5 × 104 infectious units of virus for 1 hr at 37
270 °C then applied to Vero/TMPRSS2 cells. Two days post infection cell monolayers were checked
271 for GFP expression and scored as negative (fewer than 10 cells with GFP expression), weakly
272 positive (multiple small patches of GFP), positive (large patches of GFP), or strongly positive
273 (majority of the monolayer showing GFP expression) (Figure 2, Table 4). Inocula containing no
274 mAb (virus only) were used as positive controls and inocula containing antibody but no virus
275 were used as negative controls.

276 Escape from neutralization by mAbs was significantly impacted by passage of the virus. UP virus
277 was neutralized by all three of the mAb's and VO-P6 was neutralized by 2 of the 3 mAbs (Table
278 4), whereas virus passed in the presence of antiserum, VA-P6, was able to escape neutralization
279 by all three mAbs at a concentration of 5 µg/ml. Supernatant was collected from wells showing
280 GFP and from wells from the same mAb concentrations that did not have GFP. RNA was
281 extracted from the samples (each sample was collected as a pool of the two replicate wells) and

282 the spike gene was amplified using ARTIC protocol for RT-PCR. Each sample was PCR amplified

283 and sequenced in duplicate to increase confidence in rare variant detection.

mAb conc. (ug/ml)	Control no IgG		LLNL-112 5		LLNL-112 10		S309 5		S309 10		REGN10987 5		REGN10987 10	
No Virus	-	-	-	-	-	-	-	-	-	-	-	-	-	-
UP	+++	+++	-	-	-	-	+/-	+/-	+/-	+/-	-	-	-	-
VO.P6	+++	+++	-	-	-	-	++	++	++	++	-	-	-	-
VA.P6	+++	+++	++	++	-	+/-	+	+++	+	+	++	++	-	-

284

285 ***Table 4.*** *Neutralization assay comparison of mAb escape by unpassaged and passaged virus. Viral escape was measured by GFP*

286 *expression 48 h post infection. Note: Wells scored as "+/-" were considered as negative for mAb escape. Data from deep Illumina*

287 *sequencing of the samples were used to identify mutations that were associated with mAb escape. These mutations were*

288 *compared to the mutations that occurred during passage in cell lines and under antiserum selection to understand if the*

289 *mutations originated during passage or appeared to arise de novo during mAb escape (Table 3). Epitope models were used to*

290 *visualize the placement of the mutations on the RBD and within the receptor binding motif (RBM) (Figure 2).*

291 The three mutations prevalent in the passaged virus (VO-P6 and VA-P6), T76I, H655Y, and

292 I1081V, were maintained at high frequency regardless of whether the virus escaped

293 neutralization but none of these mutations were detected in the UP samples. Similarly, the

294 I569S mutation was detected exclusively in neutralization samples derived from VO-P6. The

295 frequency of I569S increased approximately 4 fold in the S309 samples, the only mAb for which

296 neutralization escape was detected for VO-P6, but not for REGN10987 or LLNL-112 (Table 3).

297 Multiple high frequency mutations K444N, K444T, G446V, and Q493R were detected in

298 REGN10987 neutralization assay samples derived from VO-P6 (5 µg/ml) (Table 3). All of these

299 mutations have been described previously as affecting neutralization by polyclonal antiserum

300 and mAbs (25, 26). K444T and G446V were detected at the same frequency (16%) and visual

301 inspection of mapped sequencing reads revealed these mutations often co-occur and may be

302 linked.

303 Two high frequency mutations were detected in the N terminal domain (NTD) of REGN10987
304 sample VA-P6 (5 µg/ml). These mutations, H245Y (15.7%) and Y248N (17.2%), are located
305 within the NTD antigen supersite (2, 27, 28). REGN10987 is not known to bind the NTD, thus it
306 is possible these mutations are part of genotypes that have additional mutations that impact
307 REGN10987 binding such as K444T and Q493R. Both of these mutations occur in REGN10987
308 VA-P6 (5 µg/ml) sequence data at approximately the same frequency as H245Y and Y248N.
309 Visual examination of mapped sequencing reads verified that the 245 and 248 mutations are
310 linked, however, most of the Illumina reads were too short to determine if 444 and 493
311 mutations are linked.

312 Significant GFP expression was detected in all wells of the mAb S309 neutralization assay except
313 for those of the UP inoculum (Table 4, Supp Fig 2). The mutations associated with escape from
314 S309 differed between VO-P6 and VA-P6 with no high frequency mutations detected in RBD for
315 sequences from VO-P6, but an E340A mutation was detected at 57% and 30% frequency in the
316 sequences from 5 µg/ml and 10 µg/ml wells. Additional mutations at sites associated with mAb,
317 R346S and Q493R were also detected at 1% in sequence data derived from the 5 µg/ml and 10
318 µg/ml wells. Interestingly sequence data from VO-P6 wells showed three high frequency
319 mutations in the S2 spike subunit, L977F, S982L, and V991A, detected at 18%, 14%, and 16%,
320 respectively. Mutations at two of these residues, S982 and V991, may impact the positioning of
321 the RBD and thus impact infectivity (29-31).

322

323 ***Figure 2.*** *Molecular surfaces for the epitope regions for neutralizing antibodies and amino acids that are prevalent in genotypes*
324 *that escaped antibody neutralization. The epitopes are outlined and colored by degree of buried surface in the antibody-antigen*

325 *complex. The black outlined region encloses all atoms in any residue that has any atom within 5 Å of any atom of the antibody*
326 *and contributes to the molecular surface. A) REGN10987 epitope mapping shows two amino acid locations at which escape*
327 *mutations occur, 444 and 446, are in the epitope; K444 and G446 have a high buried surface area in the complex with*
328 *REGN10987, thus mutations at these positions could have high impact on the intermolecular interaction. B) LLNL-112 epitope*
329 *mapping shows the location of escape mutations (346 and 444) occur in the epitope, and K444 is highly buried in the complex. C)*
330 *Molecular surfaces for the epitope regions for S309 and amino acids prevalent in genotypes that escape S309, E340A and R346S.*
331 *E340A is in the center of the epitope and has significant buried surface in the complex. These figures were generated using*
332 *Chimera (21) and GIMP (The GIMP Development Team, 2019. GIMP, Available at: https://www.gimp.org).*

333 LLNL-112 mAb had a neutralization pattern similar to that of REGN10987 with UP and VO-P6
334 neutralized by the mAb but escape observed with VA-P6 (Tables 3 and 4). Deep sequencing
335 data showed that three RBD mutations were present in the viral RNA amplified from the 5
336 µg/ml and 10 µg/ml mAb wells. The R346S mutation was detected in the 5 µg/ml mAb wells at
337 57% frequency, whereas the 10 µg/ml wells produced different mutations, K444N at 52%
338 frequency, and Q493R at 58% for 10 µg/ml. Notably, the 10 µg/ml wells were scored as
339 negative for viral escape because fewer than 10 GFP positive cells were present, however, the
340 few cells expressing GFP were able to produce enough virus to be detectable by RT-PCR.

341 3.5 De novo mutations in RBD. Many of the mutations that were detected in the RBD at high
342 frequency after mAb selection were not detected in the viral inoculum used in the
343 neutralization assay, even when examining the samples using deep sequencing (detection of
344 mutations present at less than 1% frequency). In particular, mutations E340A, R346S, K444N,
345 K444T, G446V, and Q493R were detected at high frequencies ranging from 16 to 58% in
346 sequences generated from mAb challenged with VA-P6 (Table 3). Deep sequence analysis of
347 VA-P6 revealed that only R346S was present in VA-P6 at 1.4%, whereas the other five mutations

348 were not detected at even very low frequency and thus appear to have been generated de
349 novo, even in the case of VA-P6 inoculum with 10 µg/ml LLNL-112 mAb which had only a few
350 cells expressing GFP. Further examination of the sequence data from the six mutations showed
351 that in each case the amino acid change was due to a single nucleotide mutation, thus requiring
352 a single replication error to generate the amino acid change. These data suggest that RBD
353 escape mutants can rapidly arise de novo and be enriched to become high frequency or
354 consensus mutations.

355 3.6 Protein structure analysis of mutations. The high frequency mutations associated with
356 cell passage, antiserum selection, or antibody escape were modeled to assess potential impact
357 on protein function and antibody binding. Figure 3 shows the relative positions of a subset the
358 mutations that arose during passage. Notably, although H655Y and I1081V appear to be linked,
359 these mutations are not co-located on the spike trimer. Although previous studies have shown
360 that H655Y is frequently detected during passage and in variant genotypes (11, 16, 32), the co-
361 occurrence of I1081V has not been documented. Similarly, mutation I569S was selected for
362 during virus only passage but has not been described in the literature. Figure 3 shows the
363 position of I569S is not adjacent to the RBD on the trimer relative to the RBD. Unfortunately,
364 the residues from the furin cleavage site (681-685) are missing in all experimentally solved spike
365 structures deposited in PDB. Judging from the approximate location of this site based on
366 predicted models, residue 569 is quite far from this site and it is unlikely that I569S may directly
367 affect the cleavage site.

368

369 ***Figure 3.*** *Trimer assembly of the Spike protein with select mutations*

370

371 Protein structural models of RBD-mAb complexes were constructed to evaluate binding affinity
372 changes of mutations observed in the RBD domain and confirm whether the mutations that
373 occurred during passage with antiserum selection pressure could confer resistance to mAbs
374 (Table 5). A higher positive value for a ΔΔG scores indicates that the RBD mutant is weakening
375 (or breaking) the binding of the mAb. The predicted changes in ΔΔG agree with observed
376 mutant frequencies in 24/27 cases (85%). Indeed, the estimated ΔΔG values show an increase
377 in all positions with mutations when mutations are within RBD-mAb interface (distances
378 between RBD and mAb are below 7 Ångstroms). Thus, the results from the ΔΔG calculations
379 (Table 5) support the hypothesis that the mutations are in fact antibody escape mutations.

	E340A	R346S	K378E	L390F	K444N	K444T	G446V	T478K	Q493R
LLNL-112									
LLNL-112_AB_5		56.7%							
LLNL-112_AB_10					52.2%				58.4%
LLNL-112 ΔΔG	0	1.4	0	0	2.3	2.9	-0.7	0	0
(RBD-mAb distance)	(9.6)	(2.1)	(25.1)	(30.7)	(2.7)	(2.7)	(2.9)	(16.7)	(3.5)
REGN10987									
REGN10987_AB_5					31.2%	16.0%	40.8%		16.0%
REGN10987 ΔΔG	0	0	0	0	0.5	0.7	0.6	0	0
(RBD-mAb distance)	(13.2)	(3.0)	(20.5)	(32.4)	(3.3)	(3.3)	(2.7)	(31.1)	(11.9)
S309									
S309_AB_5	57.1%	1.1%							
S309_AB_10	30.0%								1.1%
S309 ΔΔG	3.4	2.9	0	0	-0.2	-0.2	0	0	0
(RBD-mAb distance)	(2.8)	(4.8)	(19.6)	(14.9)	(5.2)	(5.2)	(9.6)	(37.6)	(19.1)

380

381 ***Table 5.*** *Comparison of VA-P6 mutation frequencies associated with passage under mAb selection with predicted binding affinity*
382 *changes (ΔΔG) induced by observed mutations. The percent frequency of each mutation (from Table 3) is shown in the yellow-*
383 *colored rows. In each ΔΔG row (in orange) the distances (Ångstroms) between the closest atoms from the RBD mutation and*
384 *mAb interface residues are provided in parentheses.*

385 ## 4. Discussion

386 In this study, we determined that VSV/SARS-CoV-2 stock was made more genetically diverse by
387 passage under antiserum selective pressure, and that this passaged viral stock was able to more
388 readily escape monoclonal antibody neutralization as compared to unpassaged stock or viral
389 stock passaged without selective pressures. Deep sequencing detected the presence of multiple
390 mutations associated with antibody escape and enhanced transmissibility in the VSV-SARS-CoV-
391 2-S virus that had been passaged in the presence of antiserum. Analysis of mutations detected
392 in the RBD using epitope and protein structural models indicate that these mutations are a
393 result of antibody escape. These data indicate viral stock that was generated with limited
394 polyclonal antiserum selection pressure may yield more biologically relevant outcomes of
395 phenotypic assays.

396 In this and other studies (9, 33) the error prone RNA dependent RNA polymerase of the VSV
397 genome enabled rapid generation of escape mutations. Although the mutation rate of SARS-
398 CoV-2 is lower than that of other RNA viruses such as VSV that lack the 3' exonuclease
399 proofreading mechanism found in coronaviruses (34), the escape mutants observed by this and
400 other studies reflect mutations detected in natural infections (9, 33). This can be explained by
401 the large viral populations generated in natural infections and the enormous scope of the
402 CoVID-19 pandemic. A SARS-CoV-2 intrahost population is estimated to consist of over 10^9
403 copies of viral RNA (35) and this large viral population enables many different mutations to be
404 generated within a single infected individual thus increasing diversity of mutations generated in
405 natural infections (9). Thus, the rapid mutation rate of the VSV polymerase allowed us to

406 sample a larger number of mutations using a smaller population and a shorter time scale, which
407 made it possible to rapidly identify escape mutations.

408 To determine the impact of cell type on the genetic diversity of viral populations, we first
409 applied selective pressure by passing the viral stock through three different cell lines Deep
410 sequencing data indicated that passage in these cell lines induced relatively few mutations
411 present at >1%, and only one mutation, I468T detected in Caco-2 cells P4, was detected in the
412 RBD (Table 1).

413 Many of the mutations that were detected after passage in cell lines had been described in
414 prior studies. For example, a high frequency mutation, R685S, detected Vero cells P1 at 5.2%,
415 and enriched to 83.8% frequency by P4, was previously isolated from VSV/SARS-CoV-2 stock
416 (24). This mutation occurs at the S1/S2 furin cleavage site, and has also arisen previously during
417 passage of SARS-CoV-2 virus in Vero cells (36).

418 Some expected mutations such as loss of the furin cleavage site during passage in Vero cells
419 and mutation at known immune evasion site E484 were not seen (4, 32). This could be due to
420 the relatively limited number of passages in each cell line, characteristics of the antiserum used
421 for selection pressure, or the size and composition of the viral population used for the passage
422 experiments. It is possible that more extensive passage in more diverse cell lines such as cell
423 lines derived from other organs and other species might yield a more diverse set of mutations
424 (11).

425 A subset of mutations that arose during cell line passage persisted during six subsequent
426 passages in Vero/TMPRSS2 cells, with or without antiserum selection pressure (Table 3). All of

427 these persistent mutations were found at >1% frequency only in Vero/TMPRSS2 P4, and none
428 of mutations generated by passage in the other two cell lines, Vero or Caco-2, persisted. Four of
429 these mutations, L48S, T76I, H655Y, and I1081V were detected in sequences from virus passage
430 with or without the presence of antibody and escape mutant samples (Table 3). The mutations
431 at residues H655Y and I1081V were detected in the same samples and at similar frequencies,
432 thus appear to be linked. Among the four mutations consistently detected in sequences from
433 virus passage both with or without the presence of antibody, mutations T76I and H655Y are
434 present in variant of concern genotypes. Both these mutations may aid in immune escape and
435 infectivity, however, they are also associated with passage in cell culture (11, 37, 38), thus, the
436 role of these mutations in mAb escape is unclear.

437 Each of the three mAbs used in the neutralization assays was designed to neutralize SARS-CoV-
438 2 virus but differed in efficacy according to differences in variant genotypes that emerged as
439 the pandemic progressed (3). Commercially available mAbs REGN10987 (Imdevimab) and S309
440 (Sotrovimab) had been found to be sensitive to different mutations (3), and mutations in
441 Omicron subvariants have rendered both REGN10987 and S309 ineffective or weakly active
442 (39).

443 Neutralization patterns were similar for REGN10987 and LLNL-112, with both of these mAbs
444 blocking viral replication for UP and VO-P6; only VA-P6 escaped and generated significant
445 infection in the 5 µg/ml wells. The mutations generated during viral replication occurred at RBD
446 residues associated with polyclonal antiserum and mAb escape (25, 26), and within or adjacent
447 to the known epitopes of the antibodies (3) (Fig 2). Mutations at these residues (346, 444, 446,
448 and 493) have been detected in variants of concern including Omicron sublineages (40).

449 Compared to REGN10987 and LLNL-112, mAb S309 was less effective in blocking the virus
450 present in the VO-P6 and VA-P6 inoculum from entering cells but did block the viral population
451 in the UP inoculum from productively replicating in cells. Interestingly, despite the presence of
452 extensive GFP expression in VO-P6 wells, no high frequency mutations were detected in the
453 RBD, thus breakthrough may have been driven by mutations in other regions of the spike
454 protein that increased viral infectivity. Mutations S982L and V991A may impact infectivity (29,
455 31) and were detected only in the VO-P6, 10 µg/ml mAb sample, however, the viral sequences
456 derived from the VO-P6, 5 µg/ml mAb sample had different S2 subunit mutations, L977F and
457 N978K. Additionally, the I569S mutation is greatly enriched in the VO-P6 samples as compared
458 to VO-P6 samples from REGB10987 and LLNL-112 (Table 3). It is unclear if this mutation plays a
459 role in infectivity or immune evasion in vitro or in vivo; a query of outbreak.info (41) shows that
460 this mutation is rarely is detected in human sequences. S309 escape by VA-P6 appears to be
461 driven by E340A mutation was detected at high frequency. These data agree with previous
462 studies that identify mutation E340A as significantly impacting neutralization efficacy of S309
463 (42, 43), and epitope analysis indicates residue 340 is buried within mAb S309 epitope (Fig 2).

464 For mutations observed in the RBD domain of the spike protein we constructed structural
465 models of RBD-mAb complexes to evaluate binding affinity changes and confirm whether the
466 mutations that occurred during passage with antiserum selection pressure could confer
467 resistance to mAbs. A general grouping of antibody escape mutations can be based on their
468 direct or indirect contribution to the binding event. For example, (1) those that directly
469 interfere with the binding (changes within the interfaces) such as 346 or 444, and (2) those that
470 introduce some changes in local structure conformations outside the Ag-Ab interfaces that

471 impede the antibody's access. In the former case such mutations may work in conjunction with
472 some additional mutations. Results from protein structural analysis indicate that combinations
473 of mutations enabled antibody evasion: LLNL-112 was escaped by R346S and K444N mutations,
474 REGN10987 escaped by K444N/T and G446V, and S309 binding escaped by E340A and R346S.
475 Mutation Q493R co-occurs with other spike protein mutations and may belong to the second
476 category – indirect impact on the binding. This assumption is supported by the following four
477 observations: (1) Q493R is one of the major mutations observed in the Omicron variant of
478 COVID-19 that increased viral binding to ACE2 and knocked-out many known, circulating
479 antibodies (19), however in all tested RBD-mAb interactions a single-point mutation Q493R
480 alone is not affecting binding: $\Delta\Delta G = 0.0$, (2) Q493R mutation is outside the RBD interfaces with
481 REGN10987 (11.9 Å) and sotrovimab S309 (19.1 Å) (Figure 2, Table 5), and (3) the antibody
482 LLNL-112 was specifically designed to reduce impact of Omicron RBD's mutations at positions
483 446 and 493 on binding to the COV2-2130 (14, 19), (4) the analysis of spike protein sequences
484 reported in GISAID database indicates that mutation Q493R is highly dependent on the
485 presence of H655Y (indeed, in GISAID as of 26/03/2023 there are 6,480,423 sequences with
486 H655Y, 3,745,337 sequences with Q493R, from which 3,742,474 sequences with both
487 mutations which comprise 99.92% cases). In summary, protein structural modeling results
488 support the hypothesis that the detected mutations are in fact antibody escape mutations.

489 The lack of mAb neutralization displayed by the UP combined with the lack of genetic diversity
490 detected starkly contrasts with the neutralization capability and escape mutants generated by
491 virus stock generated using antiserum selection pressure. One advantage of using viral stock
492 with a very limited passage history, as represented by the UP stock, is the ability to compare

493 assay results between studies. Currently, low passaged stock virus is available from readily
494 obtainable sources such as BEI Resources repository, and this allows many different labs to use
495 the same viral stock. This study indicates that relatively few passages under antisera selection
496 are required to produce mutations that are consistently associated with antibody escape. The
497 antiserum used in this study is comprised of pooled human serum samples from Pfizer
498 vaccinees and is available as reference reagent from BEI Resources, thus providing resources for
499 laboratories to test antiserum selection using reagents from the same source (13). This
500 antiserum reagent was developed specifically as a general reference reagent to be used by
501 different laboratories across the globe for comparison of assay results, and data from this study
502 shows the value of this resource.

503 5. Conclusions

504 Deep sequencing of COVID-positive clinical samples obtained from immunocompromised
505 patients show the impact of a sub-neutralizing antibody response on the diversity of SARS-CoV-
506 2 intrahost viral populations (1, 44-46) and the emergence of variant genotypes. Even in
507 immunocompetent hosts that mount a rapid and robust immune response to infection to RNA
508 viruses such SARS-CoV-2, the large viral population size combined with the high genome
509 replication error rate, both which characterize RNA viruses, enable evolution of a diverse
510 mutant spectrum (47). As most recently illustrated with SARS-CoV-2, this rampant generation of
511 new genotypes within a host may enable these viruses to adapt to host immunity and
512 occasionally jump to host new species.

513 The passage protocol used in this study explored the relative impact of passage in multiple cell
514 lines followed by passage under antiserum selection pressure on the generation of variant
515 genotypes and the emergence of mAb escape mutations. Although relatively few new
516 mutations emerged after four passages in three different cell lines, passage with or without
517 antiserum selection pressure rapidly induced distinct sets of mutations. However, only viral
518 inoculum derived from antiserum selection was able to escape neutralization of three different
519 mAbs. Importantly, the viral stock that was not passaged under selection pressure (cell line or
520 antiserum) was not able to produce escape mutants. These data indicate that using viral stock
521 that has been generated under types of selection pressure that reflect the natural environment
522 of the virus may yield more biologically relevant outcomes of phenotypic assays.

523

524 Funding: This research was funded by Department of Energy, Office of Science, field work
525 proposal number SCW1700, and LDRD 20-ERD-064.

526

527 Acknowledgments: This work was performed under the auspices of the U.S. Department of
528 Energy by Lawrence Livermore National Laboratory under Contract DE-AC52-07NA27344. The
529 following reagent was obtained through BEI Resources, NIAID, NIH: Pooled Human Serum
530 Sample, Pfizer Vaccine, NRH-17727. VSV-SARS-CoV-2-S virus and Vero-TMPRSS2 cells received
531 from Sean Whelan's laboratory (Univ Washington). Antibody LLNL-112 was prepared by Bonnee
532 Rubinfield.

533

534 ## References

535 1. Avanzato VA, Matson MJ, Seifert SN, Pryce R, Williamson BN, Anzick SL, et al. Case
536 Study: Prolonged Infectious SARS-CoV-2 Shedding from an Asymptomatic Immunocompromised
537 Individual with Cancer. Cell. 2020;183(7):1901-12.e9.

538 2. Chen Y, Zhao X, Zhou H, Zhu H, Jiang S, Wang P. Broadly neutralizing antibodies to SARS-
539 CoV-2 and other human coronaviruses. Nature Reviews Immunology. 2023;23(3):189-99.

540 3. Cox M, Peacock TP, Harvey WT, Hughes J, Wright DW, Willett BJ, et al. SARS-CoV-2
541 variant evasion of monoclonal antibodies based on in vitro studies. Nat Rev Microbiol.
542 2023;21(2):112-24.

543 4. Funnell SGP, Afrough B, Baczenas JJ, Berry N, Bewley KR, Bradford R, et al. A cautionary
544 perspective regarding the isolation and serial propagation of SARS-CoV-2 in Vero cells. npj
545 Vaccines. 2021;6(1):83.

546 5. Magnus CL, Hiergeist A, Schuster P, Rohrhofer A, Medenbach J, Gessner A, et al.
547 Targeted escape of SARS-CoV-2 in vitro from monoclonal antibody S309, the precursor of
548 sotrovimab. Front Immunol. 2022;13:966236.

549 6. Ogando NS, Dalebout TJ, Zevenhoven-Dobbe JC, Limpens R, van der Meer Y, Caly L, et al.
550 SARS-coronavirus-2 replication in Vero E6 cells: replication kinetics, rapid adaptation and
551 cytopathology. J Gen Virol. 2020;101(9):925-40.

552 7. Sasaki M, Uemura K, Sato A, Toba S, Sanaki T, Maenaka K, et al. SARS-CoV-2 variants
553 with mutations at the S1/S2 cleavage site are generated in vitro during propagation in
554 TMPRSS2-deficient cells. PLOS Pathogens. 2021;17(1):e1009233.

555 8. Case JB, Rothlauf PW, Chen RE, Liu Z, Zhao H, Kim AS, et al. Neutralizing Antibody and
556 Soluble ACE2 Inhibition of a Replication-Competent VSV-SARS-CoV-2 and a Clinical Isolate of
557 SARS-CoV-2. Cell Host Microbe. 2020;28(3):475-85.e5.
558 9. Weisblum Y, Schmidt F, Zhang F, DaSilva J, Poston D, Lorenzi JC, et al. Escape from
559 neutralizing antibodies by SARS-CoV-2 spike protein variants. Elife. 2020;9:e61312.
560 10. Baczenas JJ, Andersen H, Rashid S, Yarmosh D, Puthuveetil N, Parker M, et al.
561 Propagation of SARS-CoV-2 in Calu-3 Cells to Eliminate Mutations in the Furin Cleavage Site of
562 Spike. Viruses. 2021;13(12).
563 11. Chung H, Noh JY, Koo BS, Hong JJ, Kim HK. SARS-CoV-2 mutations acquired during serial
564 passage in human cell lines are consistent with several of those found in recent natural SARS-
565 CoV-2 variants. Comput Struct Biotechnol J. 2022;20:1925-34.
566 12. Hoffmann M, Kleine-Weber H, Schroeder S, Krüger N, Herrler T, Erichsen S, et al. SARS-
567 CoV-2 Cell Entry Depends on ACE2 and TMPRSS2 and Is Blocked by a Clinically Proven Protease
568 Inhibitor. Cell. 2020;181(2):271-80.e8.
569 13. Xiang J, Katz L, Winokur PL, Chaudhary A, Bradford R, Rashid S, et al. Establishment of
570 human post-vaccination SARS-CoV-2 standard reference sera. medRxiv.
571 2022:2022.01.24.22269773.
572 14. Desautels TA, Arrildt KT, Zemla AT, Lau EY, Zhu F, Ricci D, et al. Computationally
573 restoring the potency of a clinical antibody against SARS-CoV-2 Omicron subvariants. bioRxiv.
574 2023:2022.10.21.513237.
575 15. Zost SJ, Gilchuk P, Case JB, Binshtein E, Chen RE, Nkolola JP, et al. Potently neutralizing
576 and protective human antibodies against SARS-CoV-2. Nature. 2020;584(7821):443-9.

577 16. Kimbrel J, Moon J, Avila-Herrera A, Martí JM, Thissen J, Mulakken N, et al. Multiple
578 Mutations Associated with Emergent Variants Can Be Detected as Low-Frequency Mutations in
579 Early SARS-CoV-2 Pandemic Clinical Samples. Viruses. 2022;14(12).
580 17. Li H. Aligning sequence reads, clone sequences and assembly contigs with BWA-MEM.
581 arXiv preprint arXiv:13033997. 2013.
582 18. Wilm A, Aw PPK, Bertrand D, Yeo GHT, Ong SH, Wong CH, et al. LoFreq: a sequence-
583 quality aware, ultra-sensitive variant caller for uncovering cell-population heterogeneity from
584 high-throughput sequencing datasets. Nucleic Acids Res. 2012;40(22):11189-201.
585 19. Zemla A, Desautels T, Lau EY, Zhu F, Arrildt KT, Segelke BW, et al. SARS-COV-2 Omicron
586 variant predicted to exhibit higher affinity to ACE-2 receptor and lower affinity to a large range
587 of neutralizing antibodies, using a rapid computational platform. bioRxiv.
588 2021:2021.12.16.472843.
589 20. Rohl CA, Strauss CEM, Chivian D, Baker D. Modeling structurally variable regions in
590 homologous proteins with rosetta. Proteins: Structure, Function, and Bioinformatics.
591 2004;55(3):656-77.
592 21. Pettersen EF, Goddard TD, Huang CC, Couch GS, Greenblatt DM, Meng EC, et al. UCSF
593 Chimera--a visualization system for exploratory research and analysis. J Comput Chem.
594 2004;25(13):1605-12.
595 22. Abraham MJ, Murtola T, Schulz R, Páll S, Smith JC, Hess B, et al. GROMACS: High
596 performance molecular simulations through multi-level parallelism from laptops to
597 supercomputers. SoftwareX. 2015;1-2:19-25.

598 23. Barlow KA, Ó Conchúir S, Thompson S, Suresh P, Lucas JE, Heinonen M, et al. Flex ddG:
599 Rosetta Ensemble-Based Estimation of Changes in Protein–Protein Binding Affinity upon
600 Mutation. The Journal of Physical Chemistry B. 2018;122(21):5389-99.
601 24. Puray-Chavez M, Lee N, Tenneti K, Wang Y, Vuong HR, Liu Y, et al. The Translational
602 Landscape of SARS-CoV-2-infected Cells Reveals Suppression of Innate Immune Genes. mBio.
603 2022;13(3):e0081522.
604 25. Harvey WT, Carabelli AM, Jackson B, Gupta RK, Thomson EC, Harrison EM, et al. SARS-
605 CoV-2 variants, spike mutations and immune escape. Nature Reviews Microbiology.
606 2021;19(7):409-24.
607 26. Liu Z, VanBlargan LA, Bloyet L-M, Rothlauf PW, Chen RE, Stumpf S, et al. Identification of
608 SARS-CoV-2 spike mutations that attenuate monoclonal and serum antibody neutralization. Cell
609 Host Microbe. 2021:S1931-3128(21)00044-5.
610 27. Cerutti G, Guo Y, Zhou T, Gorman J, Lee M, Rapp M, et al. Potent SARS-CoV-2
611 neutralizing antibodies directed against spike N-terminal domain target a single supersite. Cell
612 Host Microbe. 2021;29(5):819-33.e7.
613 28. McCallum M, De Marco A, Lempp FA, Tortorici MA, Pinto D, Walls AC, et al. N-terminal
614 domain antigenic mapping reveals a site of vulnerability for SARS-CoV-2. Cell.
615 2021;184(9):2332-47.e16.
616 29. Baig MS, Reyaz E, Selvapandiyan A, Krishnan A. Differential binding of SARS-CoV-2 Spike
617 protein variants to its cognate receptor hACE2 using molecular modeling based binding
618 analysis. Bioinformation. 2021;17(2):337-47.

619 30. Gobeil SMC, Janowska K, McDowell S, Mansouri K, Parks R, Stalls V, et al. Effect of
620 natural mutations of SARS-CoV-2 on spike structure, conformation, and antigenicity. Science
621 (New York, NY). 2021;373(6555):eabi6226.
622 31. Mannar D, Saville JW, Sun Z, Zhu X, Marti MM, Srivastava SS, et al. SARS-CoV-2 variants
623 of concern: spike protein mutational analysis and epitope for broad neutralization. Nature
624 Communications. 2022;13(1):4696.
625 32. Amicone M, Borges V, Alves MJ, Isidro J, Zé-Zé L, Duarte S, et al. Mutation rate of SARS-
626 CoV-2 and emergence of mutators during experimental evolution. Evolution, Medicine, and
627 Public Health. 2022;10(1):142-55.
628 33. Stefan MA, Light YK, Schwedler JL, McIlroy PR, Courtney CM, Saada EA, et al.
629 Development of potent and effective synthetic SARS-CoV-2 neutralizing nanobodies. MAbs.
630 2021;13(1):1958663.
631 34. Markov PV, Ghafari M, Beer M, Lythgoe K, Simmonds P, Stilianakis NI, et al. The
632 evolution of SARS-CoV-2. Nature Reviews Microbiology. 2023;21(6):361-79.
633 35. Wölfel R, Corman VM, Guggemos W, Seilmaier M, Zange S, Müller MA, et al. Virological
634 assessment of hospitalized patients with COVID-2019. Nature. 2020;581(7809):465-9.
635 36. Kim Y, Jang G, Lee D, Kim N, Seon JW, Kim Y-h, et al. Trypsin enhances SARS-CoV-2
636 infection by facilitating viral entry. Archives of Virology. 2022;167(2):441-58.
637 37. Kimura I, Kosugi Y, Wu J, Zahradnik J, Yamasoba D, Butlertanaka EP, et al. The SARS-CoV-
638 2 Lambda variant exhibits enhanced infectivity and immune resistance. Cell Rep.
639 2022;38(2):110218.

640 38. Tian D, Sun Y, Zhou J, Ye Q. The global epidemic of SARS-CoV-2 variants and their
641 mutational immune escape. J Med Virol. 2022;94(3):847-57.
642 39. Planas D, Bruel T, Staropoli I, Guivel-Benhassine F, Porrot F, Maes P, et al. Resistance of
643 Omicron subvariants BA.2.75.2, BA.4.6, and BQ.1.1 to neutralizing antibodies. Nature
644 Communications. 2023;14(1):824.
645 40. Cao W-C, Liu W, Zhang P-H, Zhang F, Richardus JH. Disappearance of Antibodies to SARS-
646 Associated Coronavirus after Recovery. N Engl J Med 2007;357(11):1162-3.
647 41. Gangavarapu K, Latif AA, Mullen JL, Alkuzweny M, Hufbauer E, Tsueng G, et al.
648 Outbreak.info genomic reports: scalable and dynamic surveillance of SARS-CoV-2 variants and
649 mutations. Nature Methods. 2023;20(4):512-22.
650 42. Cathcart AL, Havenar-Daughton C, Lempp FA, Ma D, Schmid MA, Agostini ML, et al. The
651 dual function monoclonal antibodies VIR-7831 and VIR-7832 demonstrate potent in vitro and in
652 vivo activity against SARS-CoV-2. bioRxiv. 2022:2021.03.09.434607.
653 43. Thakur S, Sasi S, Pillai SG, Nag A, Shukla D, Singhal R, et al. SARS-CoV-2 Mutations and
654 Their Impact on Diagnostics, Therapeutics and Vaccines. Frontiers in Medicine. 2022;9.
655 44. Kemp SA, Collier DA, Datir RP, Ferreira IATM, Gayed S, Jahun A, et al. SARS-CoV-2
656 evolution during treatment of chronic infection. Nature. 2021;592(7853):277-82.
657 45. Weigang S, Fuchs J, Zimmer G, Schnepf D, Kern L, Beer J, et al. Within-host evolution of
658 SARS-CoV-2 in an immunosuppressed COVID-19 patient as a source of immune escape variants.
659 Nature Communications. 2021;12(1):6405.

660 46. Cele S, Karim F, Lustig G, San JE, Hermanus T, Tegally H, et al. SARS-CoV-2 prolonged
661 infection during advanced HIV disease evolves extensive immune escape. Cell Host Microbe.
662 2022;30(2):154-62. e5.
663 47. Moya A, Holmes EC, González-Candelas F. The population genetics and evolutionary
664 epidemiology of RNA viruses. Nat Rev Microbiol. 2004;2(4):279-88.

665

666 Supporting Information: Figure S1: Sequence read coverage depth for sequences derived from
667 neutralization assay.; Figure S2: Neutralization assay, GFP expression results.; Figure S3:
668 Comparison of epitope regions for three SARS-CoV-2 neutralizing antibodies and the hACE2
669 receptor binding motif (RBM).; Table S1: Mutation distribution among samples passaged with
670 or without antibody selection pressure.

671

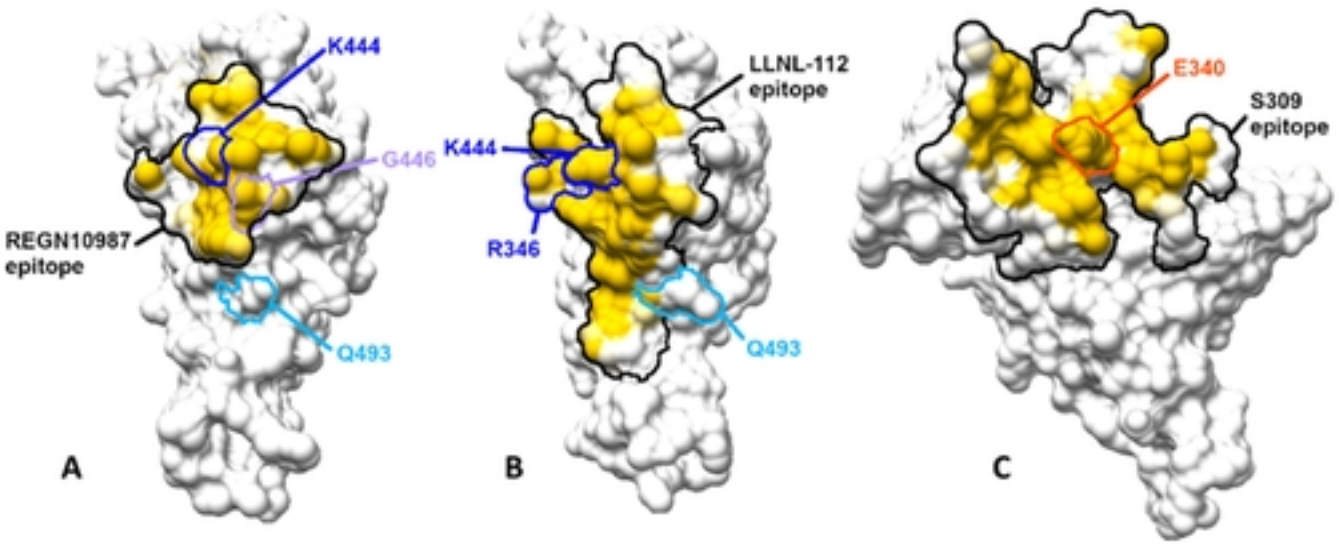
K444
G446
REGN10987
epitope
Q493
A
K444
R346
LLNL-112
epitope
Q493
B
E340
S309
epitope
C

Figure 2

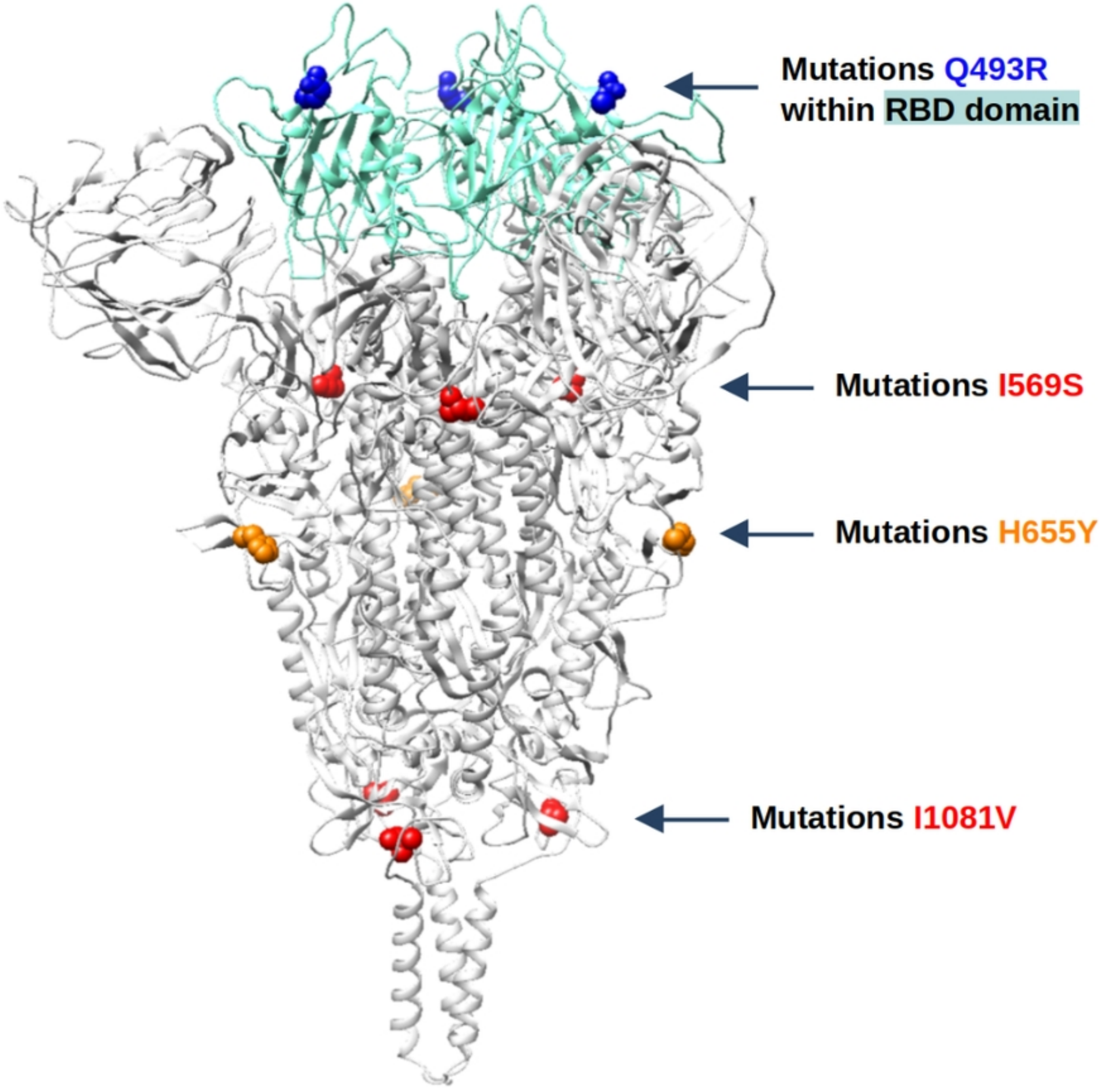
Mutations Q493R
within RBD domain
Mutations I569S
Mutations H655Y
Mutations I1081V

Figure 3

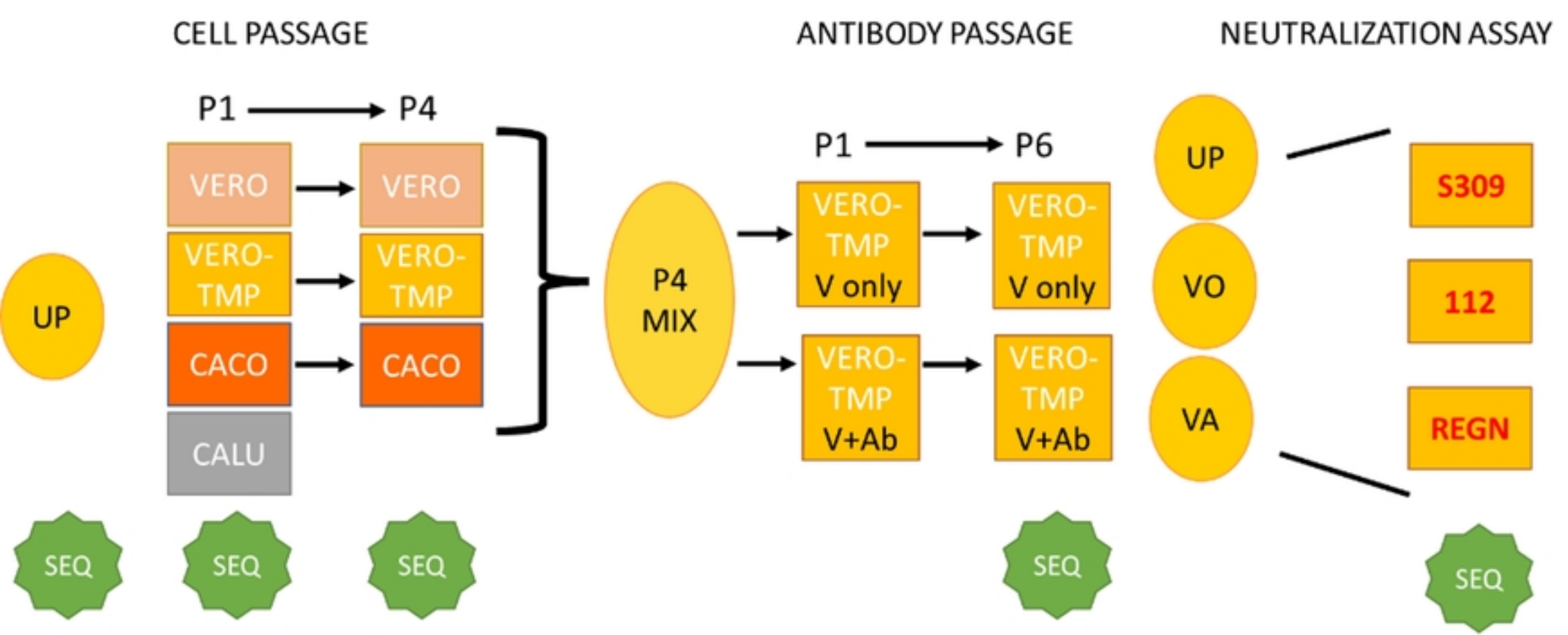
CELL PASSAGE
ANTIBODY PASSAGE
NEUTRALIZATION ASSAY
P1
P4
VERO
VERO
VERO-TMP
VERO-TMP
CACO
CACO
CALU
UP
P4 MIX
P1
P6
VERO-TMP V only
VERO-TMP V only
VERO-TMP V+Ab
VERO-TMP V+Ab
UP
VO
VA
S309
112
REGN
SEQ
SEQ
SEQ
SEQ
SEQ

Figure 1